Vibrational Spectroscopy 86 (2016) 270–276

Contents lists available at ScienceDirect

Vibrational Spectroscopy

journal homepage: www.elsevier.com/locate/vibspec

Temperature- and power-dependent phonon properties of suspended continuous WS_2 monolayer films☆

Anderson G. Vieira[a], Cleanio Luz-Lima[a], Gardenia S. Pinheiro[a], Zhong Lin[b], Julio A. Rodríguez-Manzo[d], Nestor Perea-López[b], Ana Laura Elías[b], Marija Drndić[d], Mauricio Terrones[b], Humberto Terrones[c], Bartolomeu C. Viana[a,*]

[a] Departamento de Física, Campus Ministro Petrônio Portella, Universidade Federal do Piauí, CEP 64.049-550 Teresina, PI, Brazil
[b] Department of Physics and Center for 2-Dimensional and Layered Materials, The Pennsylvania State University, University Park, PA 16802, USA
[c] Department of Physics, Applied Physics and Astronomy, Rensselaer Polytechnic Institute, 110 Eighth Street, Troy, NY 12180, USA
[d] Department of Physics and Astronomy, University of Pennsylvania, Philadelphia, Pennsylvania 19104, USA

ARTICLE INFO

Article history:
Received 1 April 2016
Received in revised form 9 August 2016
Accepted 9 August 2016
Available online 10 August 2016

Keywords:
TMDs
WS_2
Raman spectroscopy
Thermal conductivity

ABSTRACT

This manuscript reports temperature- and power-dependence of in-plane E^1_{2g} and out-of-plane A_{1g} Raman modes in a continuous WS_2 monolayer film (CWMF) prepared using low pressure chemical vapor deposition (LPCVD), suspended on a perforated substrate. The frequencies of these two phonon modes vary linearly with temperature (77–523 K) and power (2–14 μW), and the modes soften as local temperature increases. The first-order temperature coefficients for E^1_{2g} and A_{1g} modes are 0.0124 and 0.0112 cm^{-1}/K, respectively, and power coefficients are 0.1228 and 0.1381 cm^{-1}/μW. Using the 1D Balandin's approach, we have calculated the thermal conductivity of the suspended CWMF at room temperature to be *ca.* 20 and 16 W/mK when considering the E^1_{2g} and A_{1g} modes, respectively. Our results provide thermal properties values of CWMF, which are very important for developing monolayer WS_2 electronic devices.

1. Introduction

Single-layer transition metal dichalcogenides (TMDs), in particular MoS_2 and WS_2, have attracted the interest of scientists worldwide due to their remarkable optical and eletronic properties, which offer the possibility of flexible and transparent electronic devices, since these materials could be used in low-power optoeletronic and valleytronics devices, photo-sensors and other applications [1–10]. Single-layer TMDs feld-effect transistors are expected to have high an on/off ratio related to the band gap of 1.0–2.0 eV and the charge mobility can be altered by changing the gate material [11,12]. An indirect to direct band gap transition when the TMDs are thinned to single-layer was found, which provides new opportunities for electronic structure engineering of TMDs at the nanometric scale [13,14]. For example, bulk WS_2 is an indirect semiconductor material and when it is thin to a single-layer sheet, the band gap becomes wider and direct at ~2.1 eV. This is an effect of the quantum confinement, which affects the electronic and optical properties and increases the possibility to use WS_2 nanosheets in various optoeletronic devices [15]. Furthermore, the band gap of single-layer TMDs can be tuned reversibly by biaxial strain and to be able capturing a broad range of the visible spectrum [16]. Besides these remarkable properties, single-layer TMDs are also a useful materials for spintronics and valleytronics [6,17]. All these cited applications are related to the thermal properties. For instance, an efficient heat dissipation is necessary to promote a high-performance on electronic devices, while low heat dissipation is preferred in thermoelectric applications. Therefore, it is extremely necessary to understand the thermal transport properties of mono and few-layered TMDs [18]. Thus, we can conclude from all these interesting properties revealed that WS_2 is a potential candidate for next generation electronic device applications in nanotechnology.

The study of the vibrational properties of CWMF is important to understand the transport properties and the electron–phonon interactions, which are intimately related to the performance of electronic devices. Vibrational properties are also important to understand non-harmonic effects in the lattice potential energy. Furthermore, the electronic devices performance depends on the characteristic of the heat dissipation and thermal conductivity.

☆ Selected paper from for IV Encontro Brasileiro de Espectroscopia Raman (EnBraER), in Juiz de Fora, December 06–09, 2015.

* Corresponding author.
E-mail address: bartolomeu@ufpi.edu.br (B.C. Viana).

http://dx.doi.org/10.1016/j.vibspec.2016.08.004
0924-2031/

Thus, a better understanding on the changes observed in Raman spectroscopy band positions with temperature is needed to infer about the thermal properties of this very important 2D material. Raman spectroscopy is widely used non-destructive characterization technique used to measure the number of atomic layers and thermal properties of graphene, as well as different inorganic layered materials [19–29]. There are many reports about the thermal properties of suspended and supported TMDs layers showing the influence of the substrate [25,27,29–32]. However, results about WS_2 monolayers, which were grown by ambient pressure CVD (APCVD) and exfoliated mechanically (from single-crystal samples), showed different values of thermal properties and do not mention any measurements on suspended continuous monolayer film, which is a film polycrystalline containing grain boundaries which can play an important role in the thermal properties influencing transport properties [25,31,33]. The CWMF is very large (area > 1 cm^2) when compared with monolayer single crystals (triangles or hexagons, area < 1 mm^2) and the crystalline domains of CWMF are nanosized which can show different thermal properties providing an important input for applications of this material. Besides, the large disparity of the thermal properties which were theoretically predicted also motivates further experimental investigations [18,29,34,35]. Thus, to the best of our knowledge, temperature- and power-dependent Raman spectroscopy of a CWMF has not been reported hitherto until now and to understand the thermal properties of this large film it is very important for the future of applications using these 2D material.

Here, we report for the first time a temperature- and power-dependent study of the vibrational modes for suspended CWMF grown by LPCVD technique, using Raman spectroscopy, and to determine their thermal properties [36]. The power-dependence has been performed by the laser heating of the suspended sample (different from the supported flake used in M and Late work) and monitoring the frequency shift of the phonon mode. By analyzing the changes of modes in both temperature- and power-dependent measurements, the thermal conductivity of suspended CWMF was estimated and when we compared with the results of Peimyoo et al. (WS_2 monolayer exfoliated from single-crystals), we noticed a decrease in thermal conductivity values, probably, from the grain boundaries effects into the CWMF [31]. These results provide a fundamental information about the heat dissipation in the CWMF, which is useful for thermal management in various electronic applications.

2. Experimental

The large area WS_2 monolayer films (>1 cm^2) were synthesized on a SiO_2/Si substrate using a two-step process which is described by Elías et al. [36]. Then, the WS_2 films were transferred from the original Si/SiO_2 wafer to a drilled SiN/Si grid using PMMA process as it was described previously by Elias et al. [36]. The SiN has holes of 5–10 μm in diameter drilled by focus ion beam (FIB) attached to a SEM microscope. Two different samples were produced and transferred to get a good reproducibility of the experiments.

SEM observations were carried out in a Philips XL30 operated at 20 kV. Non-contact atomic force microscopy (AFM) was performed using a MFP-3D-SA from Asylum Research. WS_2 films were also characterized by Raman spectroscopy using a Renishaw inVia confocal microscope-based spectrometer with the 488 and 514.5 nm laser excitations; laser power was kept under 20 μW to avoid possible heating effect when using the back scattering geometry. The 520.5 cm^{-1} phonon mode from silicon was used for calibration. A 100× objective lens and with a numeric aperture of NA = 0.95 was used to focus the laser beam and to collect the Raman signal. For the Raman mapping acquisition, both the excitation and collection optics remained fixed while the sample was moved in x and y axis. The temperature-dependent measurements were performed using a Linkam thermal stage THMS600, a 50× lens with NA = 0.50 and the line 488 nm was used for exciting the Raman spectrum. For the power-dependent measurements,

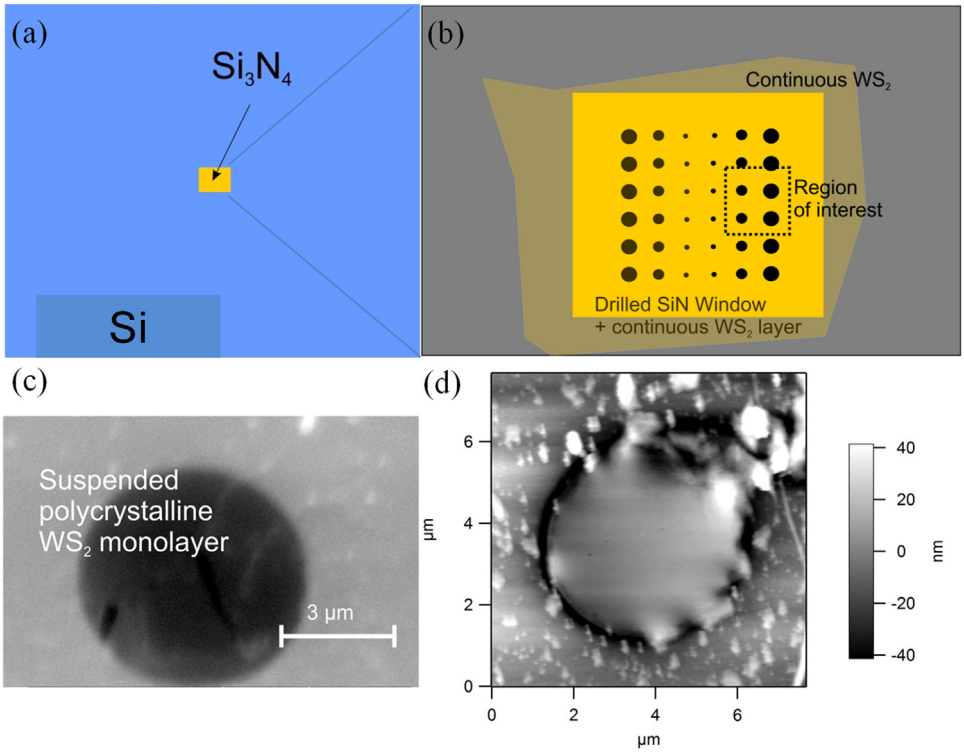

Fig. 1. (a) Schematics of the SiN drilled window in the Si chip. (b) Schematics of the SiN drilled window with CWMF suspended on the holes. (c) SEM image recorded from the CWMF suspended on the hole. (d) AFM image performed on the WS_2 monolayer film suspended.

the 100× lens and 488 nm laser line were used. The spectrometer slit was set for a resolution of 2 cm^{-1}. The size of the holes is sufficiently large to allow the extraction of the monolayer WS_2 thermal conductivity with high accuracy, because its diameter (5–10 μm) is much larger than the laser beam spot size (<1 μm). The laser beam and the hole sizes are important parameters for acquiring with high accuracy the thermal properties.

The Raman measurements were performed in several different holes of the samples and the reproducibility is really good, because the data resolution (<1 cm^{-1}) was kept below of the error resolution of the setup. Furthermore, it was used the average data of different holes to extract the fittings of the temperature e power dependency results.

3. Results and discussions

Fig. 1(a) shows the schematic diagram of the chip setup, the silicon chip with the Si_3N_4 (SiN) window where it was deposited the WS_2 film synthesized. Fig. 1(b) shows the diagram of the SiN window drilled using focused ion beam (FIB) with the CWMF on the holes. Fig. 1(c) shows a scanning electron microscope (SEM) image of the WS_2 sheet on the hole (~6 μm of diameter) of SiN window which corresponds to the region shown in Fig. 1(a) and used to perform the Raman measurements. Fig. 1(d) shows the AFM image of CWMF and the thickness of the sheet was ~0.8 nm which indicates the monolayer nature of WS_2 [36]. WS_2 few layers show a Raman modes position dependence of the in-plane (E^1_{2g}) and out-of-plane (A_{1g}) along with both modes shifting away from each other in frequency with increasing of the number of layers which can be the spectral finger-print of WS_2 monolayer [21]. Fig. 2(a) shows the Raman spectra of the WS_2 film synthesized on SiO_2/Si recorded at room temperature using 488 and 514.5 nm laser excitation. Raman spectra of CWMF are typical of monolayer film samples and are in good agreement with that reported earlier by Elias et al. [36]. When it was excited using 488 nm, Raman active modes of bulk WS_2 comprise of A_{1g}, E_{1g}, E^1_{2g}, and E^2_{2g} at the centre of the Brillouin zone, but E_{1g} is forbidden in our back-scattering configuration, and the E^2_{2g} mode is less studied due to its low frequency out of most conventional Raman spectral ranges [21,37]. Note that, according to group theory analysis, the precise assignments of Raman modes in single-layer, bilayer and bulk WS_2 should be different [38]. In this work, we used the same notation of A_{1g} (Γ) and E^1_{2g}(Γ) for single-layer, bilayer and bulk WS_2. A_{1g} (Γ) and E^1_{2g}(Γ) modes for single-layer area assigned as an out-of-plane vibrational mode of sulphur atoms, and an in-plane vibrational mode (see inset of Fig. 2a), respectively. At 514.5 nm, a dominant 2LA(M) mode was observed overlapping with E^1_{2g} mode, as reported before [21,36,37,39]. Moreover, other Raman modes are attributed to combination modes [39]. The highest intensity of the 2LA(M) mode at 514.5 nm is related with the double resonance process in WS_2 monolayer [21]. Thus, Raman spectra can be used as a fast approach to identify the number of layers of WS_2. Fig. 2b shows a schematic diagram of the experimental setup which it was performed the Raman measurements in the center of the film on the hole (suspended sample) and in the film out of the hole (supported sample). Moreover, the Raman measurements performed on WS_2 suspended and supported films have shown small shifts of the A_{1g} (Γ) and E^1_{2g}(Γ) modes and this shift is an effect of the substrate, probably, promoting strain which can affect those modes, respectively [40,41]. However, more investigation is needed to clarify the effect of the substrate. The previous studies on suspended and supported TMDs layers show that the substrate has a negligible effect on the temperature coefficients of Raman modes [27,31,32]. But, the substrate has influenced the heat dissipation due to the phonon leakage in the substrate and vicinities as observed for supported graphene and other TMDs samples [22,29,31,32]. Thus, the laser-induced heat flows radially from the centre of the suspended CWMF towards the edge of the hole and laser beam sizes are important parameters to infer about the thermal dissipation. In our case, the size of hole used is ~6 μm in diameter (Fig. (c)), which is much larger than the spot size of the laser (~0.4 μm).

Temperature-dependent Raman measurements of suspended CWMF were performed at 77–523 K using 488 nm laser as the excitation source. Fig. 3(a) shows normalized Raman spectra of suspended sample in the region of E^1_{2g}(Γ) and A_{1g}(Γ) collected at

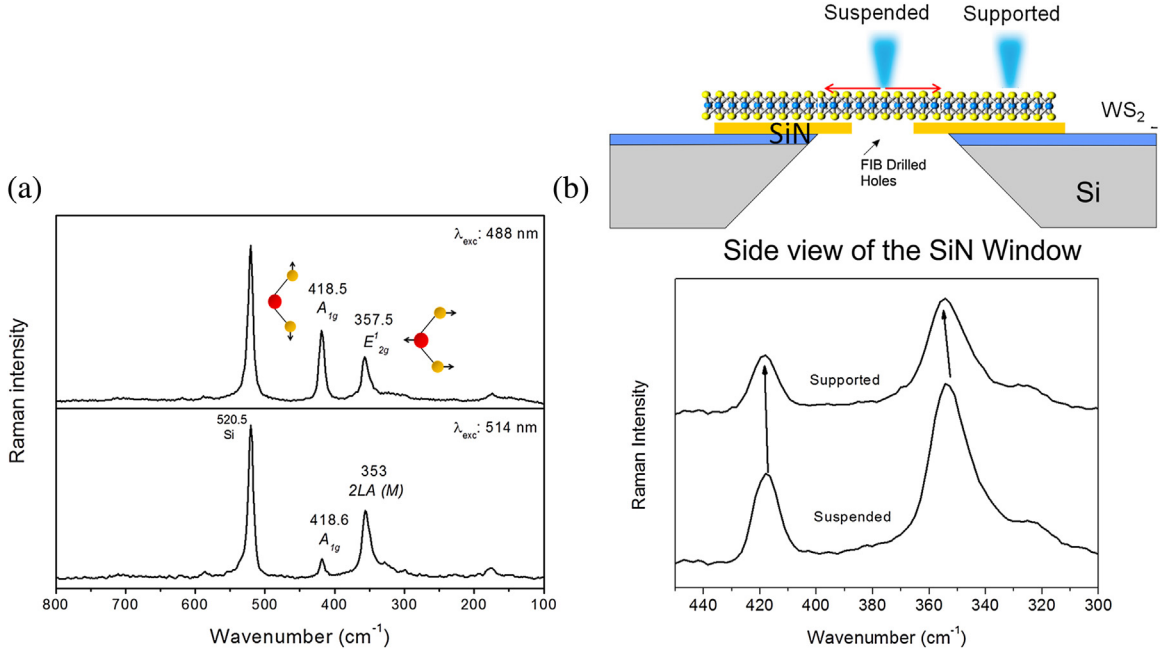

Fig. 2. (a) Room temperature Raman spectra of the CWMF using 488 nm and 514.5 nm as laser excitation. (b) Schematics of the experimental setup for suspended and supported film on top and Raman spectra of the continuous WS_2 monolayer film suspended and supported on the SiN.

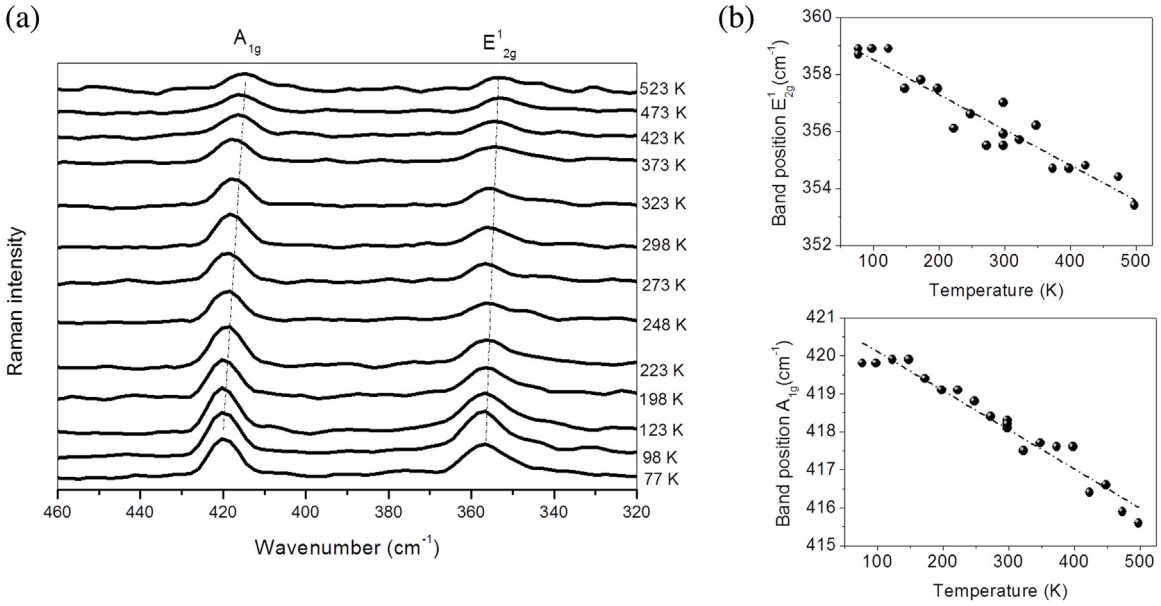

Fig. 3. (a) Raman spectra of CWMF suspended recorded at different temperatures. (b) Temperature-dependence of the wavenumbers of Raman active E^1_{2g} (top) and A_{1g} (bottom) modes in CWMF suspended.

various temperatures. Only samples on the holes with the larger diameter of 5 μm were studied in order to minimize the effects from the side wall of the hole, and to ensure that the Raman signal is fully collected from the suspended monolayer rather than from the supported region. These Raman modes were fitted by Lorentzian multiple-bands and the temperature-dependence of E^1_{2g} and A_{1g} frequencies are plotted in Fig. 3(b). As expected, both modes red-shifted with the increase of temperature, analogous to what was observed in another TMDs submitted to the increase of temperature [27,29,31,32,42]. Note that the measurements have been performed several times on different holes to confirm the temperature dependence of the Raman modes.

In order to fit the experimental data we have used an anharmonic phonon decay model for the wavenumbers [43], as follows:

$$\omega = \omega_0 + \alpha\left[1 + \frac{2}{e^x - 1}\right] + \beta\left[1 + \frac{3}{e^y - 1} + \frac{3}{(e^y - 1)^2}\right] \quad (1)$$

where $x = \frac{\hbar\omega_0}{2K_BT}$, $y = \frac{\hbar\omega_0}{3K_BT}$, $\hbar$ is the Planck's constant divided by 2π, T is the absolute temperature and K_B is the Boltzmann's constant, ω is the wavenumber at T, ω_0 is the wavenumber at 0 K, α is the first-order $(\partial\omega/\partial T)$ temperature coefficient and β is the second-order temperature coefficient.

In our case, the temperature dependence of the both modes were fitted using the following linear equation (an approximation of Eq. (1)):

$$\omega(T) = \omega_0 + \alpha T, \quad (2)$$

A higher order temperature coefficient (β) was not considered because this coefficient is not relevant at the range of temperature used here (77–523 K). The slopes of the temperature-dependences extracted from the linear fitting define the α value, which are shown in Table 1. The influence of temperature on the TMDs phonon modes is twofold: The intrinsic temperature contribution due to the phonon anharmonicity, and the volume contribution caused by the thermal expansion of the layer.

It is worth to note that the linear dependence of the Raman band frequencies with temperature has also been observed in graphene and others TMDs supported and suspended [20,25,27,29,31,32,42]. By comparison, the temperature coefficients of the Raman modes of the suspended CWMF are at the same order as those for other TMDs and graphene [20,27,29,31,32,42]. However, the values of $\partial\omega/\partial T$ are twice larger than those reported by M and Late and these discrepancies with our results could be related with the temperature control and the contact between sample and heat sink in supported sample of them. However, our results are similar to the Peimyoo et al. and the slight discrepancies of the $\partial\omega/\partial T$ values could be related to the different synthesis method which provided us a polycrystalline monolayer film of WS_2 instead of single-crystals of Peimyoo et al. and the larger range of temperature used in our work (77–523 K).

Furthermore, the power-dependence of suspended CWMF have been investigated. Particularly, to obtain the intrinsic power-dependence of WS_2 layers, it is necessary to perform the measurements using suspended samples because the substrate may influence the heat dissipation due to the phonon leakage in the vicinity of interfaces between the material and the substrate as observed in supported TMDs and graphene samples [22,27,29,31]. The power-dependence and thermal conductivity of 2D materials were previously studied using Raman spectroscopy and this technique has been developed for that [20,22,27,29,31,32]. Raman spectra for the A_{1g} and E^1_{2g} modes of monolayer film of WS_2 at various laser powers are shown in Fig. 4(a). As the laser power increases, the modes intensities increase and their frequencies redshift. These changes indicate that the increase of laser power

Table 1
First-order temperature coefficients, power shift rates and room-temperature of suspended CWMF.

Raman modes	δω/δT (cm^{-1}/K)	δω/δP (cm^{-1}/μW)	K (W/mK)
E^1_{2g}	0.0124 ± 0.0009	0.1228 ± 0.0067	20 ± 2
A_{1g}	0.0112 ± 0.0005	0.1381 ± 0.0095	16 ± 1

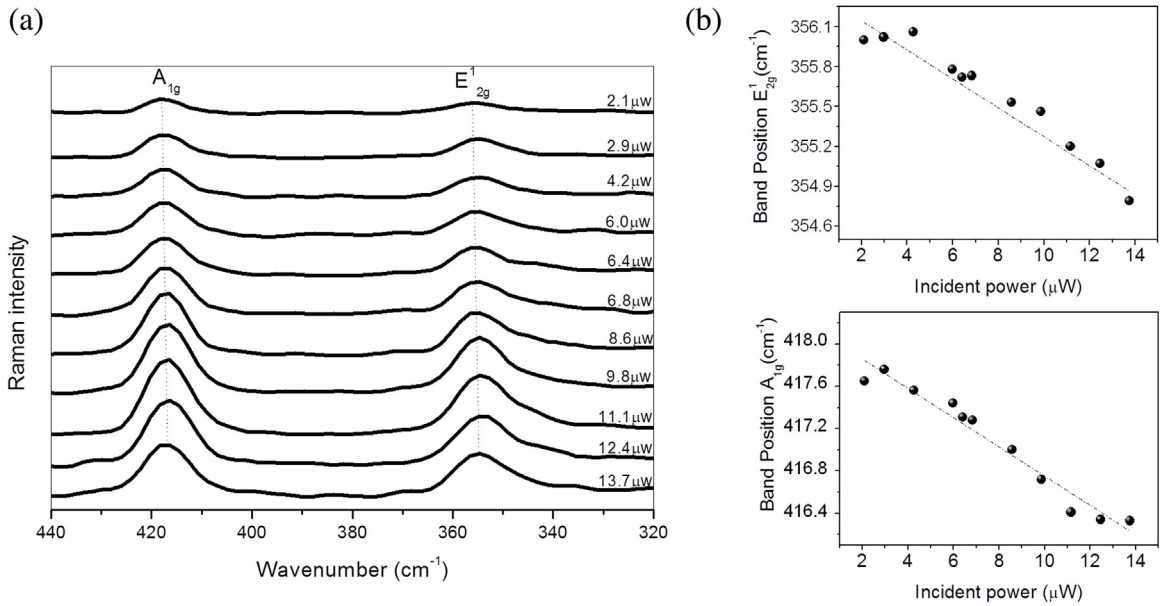

Fig. 4. (a) Raman spectra of CWMF suspended recorded at different laser powers. (b) Power-dependence of the wavenumbers of Raman active E^1_{2g} (top) and A_{1g} (bottom) modes in CWMF suspended.

has considerably increased the local temperature on the surface of sample. The power-dependences of the A_{1g} and E^1_{2g} band positions are shown in Fig. 4(b). The linear redshift of the modes reflect the local temperature rise in the film. The slopes values of $\delta\omega/\delta P$ are shown in Table 1 and the values are much larger than in the previous work with single crystals [31]. Perhaps, the high accuracy of the incident laser power measurement on the CWMF could explain the large difference between our measurements and Peimyoo et al. work. Besides, it was noticed that the laser damaging of the sample starts above 20 μW of incident power which is much smaller than the incident power used in the previous work [31].

The thermal conductivity can be evaluated by use of the experimental data from temperature- and power-dependent Raman measurements together for 2D materials [22,27,29,31]. For simplicity and just to estimate the value of thermal conductivity using our results of temperature- and power-dependence, we have used a very simple method (1D heat transport) described by Balandin et al. for graphene and useful for TMDs as well [20,27]. To extract the thermal conductivity of the CWMF, it was used the following assumptions: (i) an increase of the power will not affect the temperature of the substrate as the laser spot on CWMF is about 0.4 μm. (ii) the heat conduction is steady and uniform from the CWMF to the substrate. The expression for the heat conduction in a plane surface with cross-sectional area A can be expressed as:

$$\frac{\partial Q}{\partial t} = -k \oint \nabla T.dA, \quad ,$$

where $\frac{\partial Q}{\partial t}$ is the amount of heat transferred per second, k is thermal conductivity and T is the absolute temperature. Considering the radial heat flow from the middle of the suspended film toward its borders, Balandin et al. have derived an expression for thermal conductivity of layered materials as $k = (1/2\pi h)(\Delta P/\Delta T)$, where h is the layer thickness and ΔP is the change of laser power which generated the local temperature rise. The thermal conductivity can be written as the following approximation in one dimension heat transport.

$$K = \alpha\left(\frac{1}{2\pi h}\right)\left(\frac{\delta\omega}{\delta P}\right)^{-1} \quad (3)$$

where α is the first-order temperature coefficient of the modes and $\delta\omega/\delta P$ is the power-dependence of the phonon frequency [20,27].

Using the values of the temperature- and power-dependence Raman coefficients shown in Table 1, and the thickness of the CWMF of WS_2 ($h = 0.8$ nm) in Eq (3), the estimated thermal conductivities of the film was found for each mode and it is shown in Table 1.

Previous studies show that the thermal conductivities for suspended layered samples may be affected by the fabrication process, the determination method, the sample size (i.e. thickness and area), and the environment contamination [22,23,44]. The thermal conductivity of CWMF is comparable with those of monolayer WS_2 single-crystals grown by APCVD (32 W/mK), single-layer MoS_2 (84 W/mK) exfoliated and the recent theoretical calculations (31.8 W/mK) [19,29,31]. The chalcogenides can show phonon anharmonicities which are responsible for interesting photoinduced optical properties [45] and the knowledge about thermal conduction properties of CWMF in a very low incident power will significantly benefit to their applications as optoelectronic devices. Thus, we believe our results will be helpful in further understanding of the thermal properties of CWMF without the effect of phonon leaking on suspended materials. The possible discrepancies at the values of thermal conductivity found here, lower than others work, can be related to the grain size (nanometric) of the continuous monolayer WS_2 film which can decrease the thermal conductivity and/or possible residues of the transference process (PMMA, etc). Because of the phonon mean free path can be reduced due to the increase of phonon scattering in the intragranular region with decreasing grain size [46]. Furthermore, the difference of the k values between the two modes analyzed (in- and out-of-plane) can be an effect of strain acting differently in both modes.

4. Conclusions

We described the effects of the temperature- and power on the Raman spectroscopy studies of the in-plane E^1_{2g} and out-of-plane A_{1g} modes in a large CWMF prepared by chemical vapor deposition method on SiO_2/Si substrate and transferred to a drilled SiN substrate obtaining a suspended film. Both the E^1_{2g} and A_{1g} mode

red shift (soften) with increase of the temperature. The first-order temperature coefficients of E^1_{2g} and A_{1g} modes are found to be 0.0124 and 0.0112 cm^{-1}/K, respectively. The room-temperature thermal conductivity of suspended CWMF was obtained by performing a power-dependent Raman spectroscopy experiment and the values obtained were 0.1228 and 0.1381 $cm^{-1}/\mu W$ for E^1_{2g} and A_{1g} modes, respectively. By using the value of temperature coefficients of the modes and the data obtained from power-dependent measurements, the room-temperature thermal conductivity of CWMF was estimated to be 20 and 16 W/mK for E^1_{2g} and A_{1g} modes, respectively.

Acknowledgments

B.C. Viana, acknowledges the support from the MCTI/CNPQ/Universal 14/2013 (Grants# 471713/2013-9), and the Produtividade em Pesquisa-PQ-2013 (Grants# 303632/2013-5). C.L. Lima, also acknowledges the support from the MCTI/CNPQ/Universal 14/2014 (Grants# 454491/2014-0) and the Produtividade em Pesquisa-PQ-2013 (Grants# 306052/2014-8). We also acknowledge the support from the U.S. Army Research Office MURI grant W911NF-11-1-0362.

References

[1] N. Perea-López, Z. Lin, N.R. Pradhan, A. Iñiguez-Rábago, A. Laura Elías, A. McCreary, J. Lou, P.M. Ajayan, H. Terrones, L. Balicas, M. Terrones, CVD-grown monolayered MoS $_2$ as an effective photosensor operating at low-voltage, 2D Mater. 1 (2014) 11004, doi:http://dx.doi.org/10.1088/2053-1583/1/1/011004.

[2] M. Buscema, M. Barkelid, V. Zwiller, H.S.J. van der Zant, G.A. Steele, A. Castellanos-Gomez, Large and tunable photothermoelectric effect in single-layer MoS $_2$, Nano Lett. 13 (2013) 358–363, doi:http://dx.doi.org/10.1021/nl303321g.

[3] A.C. Ferrari, F. Bonaccorso, V. Fal'ko, K.S. Novoselov, S. Roche, P. Bøggild, S. Borini, F.H.L. Koppens, V. Palermo, N. Pugno, J.A. Garrido, R. Sordan, A. Bianco, L. Ballerini, M. Prato, E. Lidorikis, J. Kivioja, C. Marinelli, T. Ryhänen, A. Morpurgo, J.N. Coleman, V. Nicolosi, L. Colombo, A. Fert, M. Garcia-Hernandez, A. Bachtold, G.F. Schneider, F. Guinea, C. Dekker, M. Barbone, Z. Sun, C. Galiotis, A. N. Grigorenko, G. Konstantatos, A. Kis, M. Katsnelson, L. Vandersypen, A. Loiseau, V. Morandi, D. Neumaier, E. Treossi, V. Pellegrini, M. Polini, A. Tredicucci, G.M. Williams, B. Hee Hong, J.-H. Ahn, J. Min Kim, H. Zirath, B.J. van Wees, H. van der Zant, L. Occhipinti, A. Di Matteo, I.A. Kinloch, T. Seyller, E. Quesnel, X. Feng, K. Teo, N. Rupesinghe, P. Hakonen, S.R.T. Neil, Q. Tannock, T. Löfwander, J. Kinaret, Science and technology roadmap for graphene, related two-dimensional crystals, and hybrid systems, Nanoscale 7 (2015) 4598–4810, doi:http://dx.doi.org/10.1039/C4NR01600A.

[4] R. Lv, H. Terrones, A.L. Elías, N. Perea-López, H.R. Gutiérrez, E. Cruz-Silva, L.P. Rajukumar, M.S. Dresselhaus, M. Terrones, Two-dimensional transition metal dichalcogenides: clusters, ribbons, sheets and more, Nano Today 10 (2015) 559–592, doi:http://dx.doi.org/10.1016/j.nantod.2015.07.004.

[5] G.R. Bhimanapati, Z. Lin, V. Meunier, Y. Jung, J.J. Cha, S. Das, D. Xiao, Y. Son, M.S. Strano, V.R. Cooper, L. Liang, S.G. Louie, E. Ringe, W. Zhou, B.G. Sumpter, H. Terrones, F. Xia, Y. Wang, J. Zhu, D. Akinwande, N. Alem, J.A. Schuller, R.E. Schaak, M. Terrones, J.A. Robinson, Recent advances in two-dimensional materials beyond graphene, ACS Nano (2015), doi:http://dx.doi.org/10.1021/acsnano.5b05556.

[6] H. Zeng, G.-B. Liu, J. Dai, Y. Yan, B. Zhu, R. He, L. Xie, S. Xu, X. Chen, W. Yao, X. Cui, Optical signature of symmetry variations and spin-valley coupling in atomically thin tungsten dichalcogenides, Sci. Rep. 3 (2013), doi:http://dx.doi.org/10.1038/srep01608.

[7] N.R. Pradhan, J. Ludwig, Z. Lu, D. Rhodes, M.M. Bishop, K. Thirunavukkuarasu, S. A. McGill, D. Smirnov, L. Balicas, High photoresponsivity and short photoresponse times in few-layered WSe_2 transistors, ACS Appl. Mater. Interfaces 7 (2015) 12080–12088, doi:http://dx.doi.org/10.1021/acsami.5b02264.

[8] S. Hwan Lee, D. Lee, W. Sik Hwang, E. Hwang, D. Jena, W. Jong Yoo, High-performance photocurrent generation from two-dimensional WS2 field-effect transistors, Appl. Phys. Lett. 104 (2014), doi:http://dx.doi.org/10.1063/1.4878335 (193113).

[9] C. Janisch, N. Mehta, D. Ma, A.L. Elías, N. Perea-López, M. Terrones, Z. Liu, Ultrashort optical pulse characterization using WS_2 monolayers, Opt. Lett. 39 (2014) 383, doi:http://dx.doi.org/10.1364/ol.39.000383.

[10] N. Perea-López, A.L. Elías, A. Berkdemir, A. Castro-Beltran, H.R. Gutiérrez, S. Feng, R. Lv, T. Hayashi, F. López-Urías, S. Ghosh, B. Muchharla, S. Talapatra, H. Terrones, M. Terrones, Photosensor device based on few-layered WS_2 films, Adv. Funct. Mater. 23 (2013) 5511–5517, doi:http://dx.doi.org/10.1002/adfm.201300760.

[11] J. Lin, J. Zhong, S. Zhong, H. Li, H. Zhang, W. Chen, Modulating electronic transport properties of MoS2 field effect transistor by surface overlayers, Appl. Phys. Lett. 103 (2013), doi:http://dx.doi.org/10.1063/1.4818463 (63109).

[12] D. Sarkar, W. Liu, X. Xie, A.C. Anselmo, S. Mitragotri, K. Banerjee, MoS_2 field-effect transistor for next-generation label-free biosensors, ACS Nano 8 (2014) 3992–4003, doi:http://dx.doi.org/10.1021/nn5009148.

[13] H. Sahin, S. Tongay, S. Horzum, W. Fan, J. Zhou, J. Li, J. Wu, F.M. Peeters, Anomalous Raman spectra and thickness-dependent electronic properties of WSe2, Phys. Rev. B 87 (2013), doi:http://dx.doi.org/10.1103/PhysRevB.87.165409.

[14] A. Splendiani, L. Sun, Y. Zhang, T. Li, J. Kim, C.-Y. Chim, G. Galli, F. Wang, Emerging photoluminescence in monolayer MoS_2, Nano Lett. 10 (2010) 1271–1275, doi:http://dx.doi.org/10.1021/nl903868w.

[15] D.J. Late, S.N. Shirodkar, U.V. Waghmare, V.P. Dravid, C.N.R. Rao, Thermal expansion, anharmonicity and temperature-dependent Raman spectra of single- and few-layer $MoSe_2$ and WSe_2, ChemPhysChem (2014), doi:http://dx.doi.org/10.1002/cphc.201400020 (n/a-n/a).

[16] S. Tongay, W. Fan, J. Kang, J. Park, U. Koldemir, J. Suh, D.S. Narang, K. Liu, J. Ji, J. Li, R. Sinclair, J. Wu, Tuning interlayer coupling in large-area heterostructures with CVD-grown MoS $_2$ and WS $_2$ monolayers, Nano Lett. 14 (2014) 3185–3190, doi:http://dx.doi.org/10.1021/nl500515q.

[17] J. Klinovaja, D. Loss, Spintronics in MoS2 monolayer quantum wires, Phys. Rev. B 88 (2013), doi:http://dx.doi.org/10.1103/PhysRevB.88.075404.

[18] B. Peng, H. Zhang, H. Shao, Y. Xu, X. Zhang, H. Zhu, Thermal conductivity of monolayer MoS_2, $MoSe_2$, and WS_2: interplay of mass effect, interatomic bonding and anharmonicity, RSC Adv. 6 (2016) 5767–5773, doi:http://dx.doi.org/10.1039/C5RA19747C.

[19] A.A. Balandin, Phonon engineering in graphene and van der Waals materials, MRS Bull. 39 (2014) 817–823, doi:http://dx.doi.org/10.1557/mrs.2014.169.

[20] A.A. Balandin, S. Ghosh, W. Bao, I. Calizo, D. Teweldebrhan, F. Miao, C.N. Lau, Superior thermal conductivity of single-layer graphene, Nano Lett. 8 (2008) 902–907, doi:http://dx.doi.org/10.1021/nl0731872.

[21] A. Berkdemir, H.R. Gutiérrez, A.R. Botello-Méndez, N. Perea-López, A.L. Elías, C.-I. Chia, B. Wang, V.H. Crespi, F. López-Urías, J.-C. Charlier, H. Terrones, M. Terrones, Identification of individual and few layers of WS2 using Raman Spectroscopy, Sci. Rep. 3 (2013), doi:http://dx.doi.org/10.1038/srep01755.

[22] W. Cai, A.L. Moore, Y. Zhu, X. Li, S. Chen, L. Shi, R.S. Ruoff, Thermal transport in suspended and supported monolayer graphene grown by chemical vapor deposition, Nano Lett. 10 (2010) 1645–1651, doi:http://dx.doi.org/10.1021/nl9041966.

[23] S. Ghosh, W. Bao, D.L. Nika, S. Subrina, E.P. Pokatilov, C.N. Lau, A.A. Balandin, Dimensional crossover of thermal transport in few-layer graphene, Nat. Mater. 9 (2010) 555–558, doi:http://dx.doi.org/10.1038/nmat2753.

[24] H.R. Gutiérrez, N. Perea-López, A.L. Elías, A. Berkdemir, B. Wang, R. Lv, F. López-Urías, V.H. Crespi, H. Terrones, M. Terrones, Extraordinary room-temperature photoluminescence in triangular WS_2 monolayers, Nano Lett. 13 (2013) 3447–3454, doi:http://dx.doi.org/10.1021/nl3026357.

[25] M. Thripuranthaka, D.J. Late, Temperature dependent phonon shifts in single-layer WS_2, ACS Appl. Mater. Interfaces 6 (2014) 1158–1163, doi:http://dx.doi.org/10.1021/am404847d.

[26] K.S. Novoselov, Electric field effect in atomically thin carbon films, Science 306 (2004) 666–669, doi:http://dx.doi.org/10.1126/science.1102896.

[27] S. Sahoo, A.P.S. Gaur, M. Ahmadi, M.J.-F. Guinel, R.S. Katiyar, Temperature-dependent raman studies and thermal conductivity of few-layer MoS_2, J. Phys. Chem. C 117 (2013) 9042–9047, doi:http://dx.doi.org/10.1021/jp402509w.

[28] M. Thripuranthaka, R.V. Kashid, C. Sekhar Rout, D.J. Late, Temperature dependent Raman spectroscopy of chemically derived few layer MoS2 and WS2 nanosheets, Appl. Phys. Lett. 104 (81911) (2014), doi:http://dx.doi.org/10.1063/1.4866782.

[29] X. Zhang, D. Sun, Y. Li, G.-H. Lee, X. Cui, D. Chenet, Y. You, T.F. Heinz, J.C. Hone, Measurement of lateral and interfacial thermal conductivity of single- and bilayer MoS_2 and $MoSe_2$ using refined optothermal raman technique, ACS Appl. Mater. Interfaces 7 (2015) 25923–25929, doi:http://dx.doi.org/10.1021/acsami.5b08580.

[30] D.J. Late, S.N. Shirodkar, U.V. Waghmare, V.P. Dravid, C.N.R. Rao, Thermal Expansion, anharmonicity and temperature-dependent raman spectra of single- and few-layer $MoSe_2$ and WSe_2, ChemPhysChem 15 (2014) 1592–1598, doi:http://dx.doi.org/10.1002/cphc.201400020.

[31] N. Peimyoo, J. Shang, W. Yang, Y. Wang, C. Cong, T. Yu, Thermal conductivity determination of suspended mono- and bilayer WS2 by Raman spectroscopy, Nano Res. 8 (2015) 1210–1221, doi:http://dx.doi.org/10.1007/s12274-014-0602-0.

[32] R. Yan, J.R. Simpson, S. Bertolazzi, J. Brivio, M. Watson, X. Wu, A. Kis, T. Luo, A.R. Hight Walker, H.G. Xing, Thermal conductivity of monolayer molybdenum disulfide obtained from temperature-dependent raman spectroscopy, ACS Nano 8 (2014) 986–993, doi:http://dx.doi.org/10.1021/nn405826k.

[33] Y. Rong, K. He, M. Pacios, A.W. Robertson, H. Bhaskaran, J.H. Warner, Controlled preferential oxidation of grain boundaries in monolayer tungsten disulfide for direct optical imaging, ACS Nano 9 (2015) 3695–3703, doi:http://dx.doi.org/10.1021/acsnano.5b00852.

[34] X. Liu, G. Zhang, Q.-X. Pei, Y.-W. Zhang, Phonon thermal conductivity of monolayer MoS2 sheet and nanoribbons, Appl. Phys. Lett. 103 (2013) 133113, doi:http://dx.doi.org/10.1063/1.4823509.

[35] C. Muratore, V. Varshney, J.J. Gengler, J. Hu, J.E. Bultman, A.K. Roy, B.L. Farmer, A.A. Voevodin, Thermal anisotropy in nano-crystalline MoS_2 thin films, Phys.

Chem. Chem. Phys. 16 (2014) 1008–1014, doi:http://dx.doi.org/10.1039/C3CP53746C.
[36] A.L. Elías, N. Perea-López, A. Castro-Beltrán, A. Berkdemir, R. Lv, S. Feng, A.D. Long, T. Hayashi, Y.A. Kim, M. Endo, H.R. Gutiérrez, N.R. Pradhan, L. Balicas, T.E. Mallouk, F. López-Urías, H. Terrones, M. Terrones, Controlled synthesis and transfer of large-area WS_2 sheets: from single layer to few layers, ACS Nano 7 (2013) 5235–5242, doi:http://dx.doi.org/10.1021/nn400971k.
[37] C. Sourisseau, F. Cruege, M. Fouassier, M. Alba, Second-order Raman effects, inelastic neutron scattering and lattice dynamics in 2H-WS2, Chem. Phys. 150 (1991) 281–293, doi:http://dx.doi.org/10.1016/0301-0104(91)80136-6.
[38] H. Terrones, E.D. Corro, S. Feng, J.M. Poumirol, D. Rhodes, D. Smirnov, N.R. Pradhan, Z. Lin, M.A.T. Nguyen, A.L. Elías, T.E. Mallouk, L. Balicas, M.A. Pimenta, M. Terrones, New first order raman-active modes in few layered transition metal dichalcogenides, Sci. Rep. 4 (2014), doi:http://dx.doi.org/10.1038/srep04215.
[39] Y. Gong, Z. Lin, G. Ye, G. Shi, S. Feng, Y. Lei, A.L. Elías, N. Perea-Lopez, R. Vajtai, H. Terrones, Z. Liu, M. Terrones, P.M. Ajayan, Tellurium-assisted low-temperature synthesis of MoS_2 and WS_2 monolayers, ACS Nano 9 (2015) 11658–11666, doi:http://dx.doi.org/10.1021/acsnano.5b05594.
[40] S. Horzum, H. Sahin, S. Cahangirov, P. Cudazzo, A. Rubio, T. Serin, F.M. Peeters, Phonon softening and direct to indirect band gap crossover in strained single-layer MoSe2, Phys. Rev. B. 87 (2013), doi:http://dx.doi.org/10.1103/PhysRevB.87.125415.
[41] Y. Wang, C. Cong, C. Qiu, T. Yu, Raman spectroscopy study of lattice vibration and crystallographic orientation of monolayer MoS_2 under uniaxial strain, Small 9 (2013) 2857–2861, doi:http://dx.doi.org/10.1002/smll.201202876.
[42] N.A. Lanzillo, A. Glen Birdwell, M. Amani, F.J. Crowne, P.B. Shah, S. Najmaei, Z. Liu, P.M. Ajayan, J. Lou, M. Dubey, S.K. Nayak, T.P. O'Regan, Temperature-dependent phonon shifts in monolayer MoS2, Appl. Phys. Lett. 103 (93102) (2013), doi:http://dx.doi.org/10.1063/1.4819337.
[43] M. Balkanski, R.F. Wallis, E. Haro, Anharmonic effects in light scattering due to optical phonons in silicon, Phys. Rev. B 28 (1983) 1928.
[44] M.T. Pettes, I. Jo, Z. Yao, L. Shi, Influence of polymeric residue on the thermal conductivity of suspended bilayer graphene, Nano Lett. 11 (2011) 1195–1200, doi:http://dx.doi.org/10.1021/nl104156y.
[45] B. Xue, V. Nazabal, M. Piasecki, L. Calvez, A. Wojciechowski, P. Rakus, P. Czaja, I. V. Kityk, Photo-induced effects in GeS2 glass and glass-ceramics stimulated by green and IR lasers, Mater. Lett. 73 (2012) 14–16, doi:http://dx.doi.org/10.1016/j.matlet.2011.12.089.
[46] H. Dong, B. Wen, R. Melnik, Relative importance of grain boundaries and size effects in thermal conductivity of nanocrystalline materials, Sci. Rep. 4 (2014) 7037, doi:http://dx.doi.org/10.1038/srep07037.